Molecular Therapy
Original Article

Targeting the HDAC2/HNF-4A/miR-101b/AMPK Pathway Rescues Tauopathy and Dendritic Abnormalities in Alzheimer's Disease

Dan Liu,[1,2,8] Hui Tang,[1,3,8] Xin-Yan Li,[1] Man-Fei Deng,[1] Na Wei,[1] Xiong Wang,[1] Ya-Fan Zhou,[1] Ding-Qi Wang,[1] Peng Fu,[4] Jian-Zhi Wang,[3] Sébastien S. Hébert,[5,6] Jian-Guo Chen,[1,7] Youming Lu,[1] and Ling-Qiang Zhu[1,3]

[1]The Institute for Brain Research, Collaborative Innovation Center for Brain Science, Huazhong University of Science and Technology, Wuhan 430030, China; [2]Department of Medical Genetics, School of Basic Medicine, Tongji Medical College, Huazhong University of Science and Technology, Wuhan 430030, China; [3]Department of Pathophysiology, Key Laboratory of Ministry of Education for Neurological Disorders, School of Basic Medicine, Tongji Medical College, Huazhong University of Science and Technology, Wuhan 430030, China; [4]Department of Neurosurgery, Union Hospital, Tongji Medical College, Huazhong University of Science and Technology, Wuhan 430022, China; [5]Axe Neurosciences, Centre de recherche du CHU de Québec, CHUL, Québec, QC G1V 4G2, Canada; [6]Département de psychiatrie et neurosciences, Université Laval, Québec, QC G1V 0A6, Canada; [7]Department of Pharmacology, School of Basic Medicine, Tongji Medical College, Huazhong University of Science and Technology, Wuhan 430030, China

Histone deacetylase 2 (HDAC2) plays a major role in the epigenetic regulation of gene expression. Previous studies have shown that HDAC2 expression is strongly increased in Alzheimer's disease (AD), a major neurodegenerative disorder and the most common form of dementia. Moreover, previous studies have linked HDAC2 to Aβ overproduction in AD; however, its involvement in tau pathology and other memory-related functions remains unclear. Here, we show that increased HDAC2 levels strongly correlate with phosphorylated tau in a mouse model of AD. HDAC2 overexpression induced AD-like tau hyperphosphorylation and aggregation, which were accompanied by a loss of dendritic complexity and spine density. The ectopic expression of HDAC2 resulted in the deacetylation of the hepatocyte nuclear factor 4α (HNF-4A) transcription factor, which disrupted its binding to the miR-101b promoter. The suppression of miR-101b caused an upregulation of its target, AMP-activated protein kinase (AMPK). The introduction of miR-101b mimics or small interfering RNAs (siRNAs) against AMPK blocked HDAC2-induced tauopathy and dendritic impairments in vitro. Correspondingly, miR-101b mimics or AMPK siRNAs rescued tau pathology, dendritic abnormalities, and memory deficits in AD mice. Taken together, the current findings implicate the HDAC2/miR-101/AMPK pathway as a critical mediator of AD pathogenesis. These studies also highlight the importance of epigenetics in AD and provide novel therapeutic targets.

INTRODUCTION

Alzheimer's disease (AD) is the most prevalent neurodegenerative disease and is characterized by memory decline.[1] Neurofibrillary tangles (NFTs) composed of abnormally hyperphosphorylated tau proteins[2] are the major neuropathological hallmarks of AD and correlate with cognitive decline.[3] This tau-induced pathology may promote dendritic abnormalities, synaptic dysfunction, and memory impairment.[4] Thus, the alleviation of tauopathy via target-specific and disease-modifying treatments is a promising therapeutic strategy for AD.

Increasing evidence supports a role for epigenetics in AD.[5] Of the identified epigenetic modifications in the nervous system, histone acetylation has been clearly associated with the facilitation of learning and memory.[6] Reduced histone acetylation has been identified in sporadic cases of AD.[7] The acetylation of histones is predominately mediated by histone acetyltransferase (HAT) and histone deacetylase (HDAC). Pharmacological treatment with non-selective HDAC inhibitors can reverse cognitive deficits in many neurological disorders.[8] HDAC2 protein levels are strongly increased in AD brains, particularly in the entorhinal cortex and in the hippocampal CA1 area,[7] two of the earliest and most affected brain areas in AD[9] that are crucial for memory formation and storage. Interestingly, HDAC2 accumulation is initiated at Braak stages I and II, which further supports its role in the early pathogenesis of AD. However, whether and how HDAC2 directly influences tau pathology (tauopathy) and dendritic impairments to mediate memory loss remains unclear; consequently, target-specific therapeutic strategies are lacking.

Here, we first demonstrate that HDAC2 levels are positively correlated with tau hyperphosphorylation in AD mice, and the overexpression of HDAC2, in contrast to HDAC1 or HDAC3, was sufficient to promote tau hyperphosphorylation, tau aggregation, and dendritic impairments in vivo. We then show that HDAC2 overexpression

Received 20 September 2016; accepted 23 January 2017;
http://dx.doi.org/10.1016/j.ymthe.2017.01.018.

[8]These authors contributed equally to this work.

Correspondence: Ling-Qiang Zhu, Department of Pathophysiology, Tongji Medical College, Huazhong University of Science and Technology, No. 13, Hangkong Road, Wuhan 430030, China.
E-mail: zhulq@mail.hust.edu.cn

reduced the acetylation of hepatocyte nuclear factor 4α (HNF-4A), which inhibited its binding to the promoter region of miR-101b. The suppression of miR-101b leads to the upregulation of AMP-activated protein kinase (AMPK) expression at the post-transcriptional level. We subsequently antagonized this disease-modifying signal via the specific introduction of miR-101b mimics or silencing AMPK expression in cultured neurons, and we determined that tau hyperphosphorylation, aggregation, and dendritic impairments induced by HDAC2 were rescued in these cells. A similar experimental strategy rescued the behavioral abnormalities in AD mice. The current findings implicate the HDAC2/miR-101b/AMPK pathway as an important contributor to tauopathy and dendritic deficits in AD.

RESULTS

HDAC2 Levels Correlate with Phosphorylated Tau in Two Mouse Models of AD

To investigate the potential involvement of HDAC2 in the regulation of tau hyperphosphorylation, we first used 3xTg-AD mice, a widely used animal model of AD.[10] Western blot analysis indicated higher HDAC2 protein levels in 12-month-old 3xTg-AD mice but not 3-month-old 3xTg-AD mice compared with the levels in wild-type controls (Figure 1A). We subsequently measured the co-localization of HDAC2 with phosphorylated tau in the hippocampus (the CA3 region in the figures) of 12-month-old 3xTg-AD mice. Neurons that expressed nuclear HDAC2 exhibited elevated tau phosphorylation in their cytoplasm (Figures 1B–1D). Interestingly, we identified a strong positive correlation between HDAC2 and AT8 immunoreactivity (phosphorylated tau at Ser202/Thr205 sites) and a negative correlation between HDAC2 and the Tau1 epitope (non-phosphorylated tau at Ser198/199/202 sites) (Figures 1B and 1C). No correlation was identified between HDAC2 and the Tau5 epitope (total tau) (Figure 1D). Furthermore, these correlations were not present in 12-month-old wild-type littermates (data not shown). Similar correlations between HDAC2 and tau were also identified in the hippocampus of 9-month-old P301L Tau mice (Figure S1). These data suggest that HDAC2 upregulation is involved in tauopathy.

HDAC2 Overexpression Induces Tauopathy in Neurons

To determine whether excess HDAC2 directly contributes to tau pathology, we examined tau phosphorylation in mouse primary hippocampal neurons infected with lentiviruses that expressed HDAC2. We showed that HDAC2 overexpression induced tau hyperphosphorylation at several epitopes, including pS214, pT231, pS262, and AT8. As expected, Tau1 (unphosphorylated tau) was decreased (Figure 1E). Histone acetylation was decreased under these conditions, which indicates the functional expression of HDAC2 in the neurons (Figure S2). Importantly, the overexpression of HDAC1 or HDAC3 did not result in tau hyperphosphorylation (Figure S3). These results demonstrate that the specific overexpression of HDAC2 may induce tau hyperphosphorylation.

Hyperphosphorylated tau changes its conformation and aggregates inside the neuron to form toxic tau.[11] We subsequently examined the cellular distribution and aggregation properties of tau[12,13] in HEK293 cells that stably expressed human wild-type full-length (441 amino acids [aa]) tau.[14] Cells were dissociated into four fractions: cytosolic soluble tau, microtubule-bound tau, membrane-bound tau, and SDS-soluble aggregated tau. Using western blot analysis, we identified a significant enrichment (1.3-fold) of aggregated tau following HDAC2 overexpression (Figure 1F), which coincided with a 50% decrease in the level of cytosolic soluble tau. We further determined the amounts of SDS-insoluble tau aggregates using filter/trap assays.[12,15] We identified a 50% increase in detergent-resistant tau aggregates in cells transfected with HDAC2 compared with that in the control cells (Figure 1G). Taken together, these findings indicate that HDAC2 induces tau pathological changes.

In AD, tau is mislocalized to the dendritic compartment and induces synaptic alterations.[4] We subsequently aimed to determine whether HDAC2 overexpression promotes dendritic impairments in neurons. We showed that in mouse primary neurons infected with HDAC2 lentiviruses, the dendritic complexity index (DCI) values of the whole dendrite decreased by approximately 30% compared with the controls (Figures 2A and 2B). We also performed a Sholl analysis and confirmed the differences in dendritic complexity between the HDAC2- and control-infected neurons (Figure 2C). HDAC2 overexpression caused a strong reduction in spine density (from 3.71 ± 0.44 to 2.19 ± 0.53 μm^{-1}), as well as a reduction in the percentages of mushroom spines (from 36.68% ± 4.9% to 18.91% ± 4.85%) and stubby spines (from 30.08% ± 3.51% to 19.70% ± 5.30%) (Figures 2D–2G), which is consistent with previous in vivo studies.[8] Thus, in addition to tau alterations, HDAC2 upregulation causes dendritic alterations in vitro.

HDAC2 Enhances AMPK Expression via Inhibition of miR-101b

To investigate the underlying mechanisms that mediate tauopathy and dendritic impairments induced by HDAC2, we initially screened various tau kinases and phosphatases.[16] There were no changes in the levels of glycogen synthase kinase (GSK)-3, protein phosphatase 2a (PP2a), protein kinase A (PKA), and extracellular signal-regulated kinase (ERK) (Figure S4) or tau acetylation in hippocampal neurons that expressed HDAC2 (Figure S5). However, we identified a substantial increase in AMPK activity and expression (Figures 3A and 3B). In contrast, AMPK mRNA levels were not altered under these conditions (Figure 3C), which suggests a post-transcriptional mode of regulation.

Histone deacetylation typically leads to the suppression of gene expression. The somewhat contradictory effects of HDAC2 on AMPK protein (but not mRNA) levels prompted us to investigate the involvement of microRNAs (miRNAs). miRNAs may induce the translational repression of target mRNA transcripts.[17] A bioinformatic analysis identified putative binding sites for miR-101a/b, miR-130, miR-137, miR-148, and miR-19 within the 3′ UTR of AMPK mRNA (gene *PRKAA1*) (Figure S6). Using miRNA qRT-PCR, we measured candidate miRNA levels in HDAC2-overexpressing neurons and determined that a single miRNA, miR-101b, was

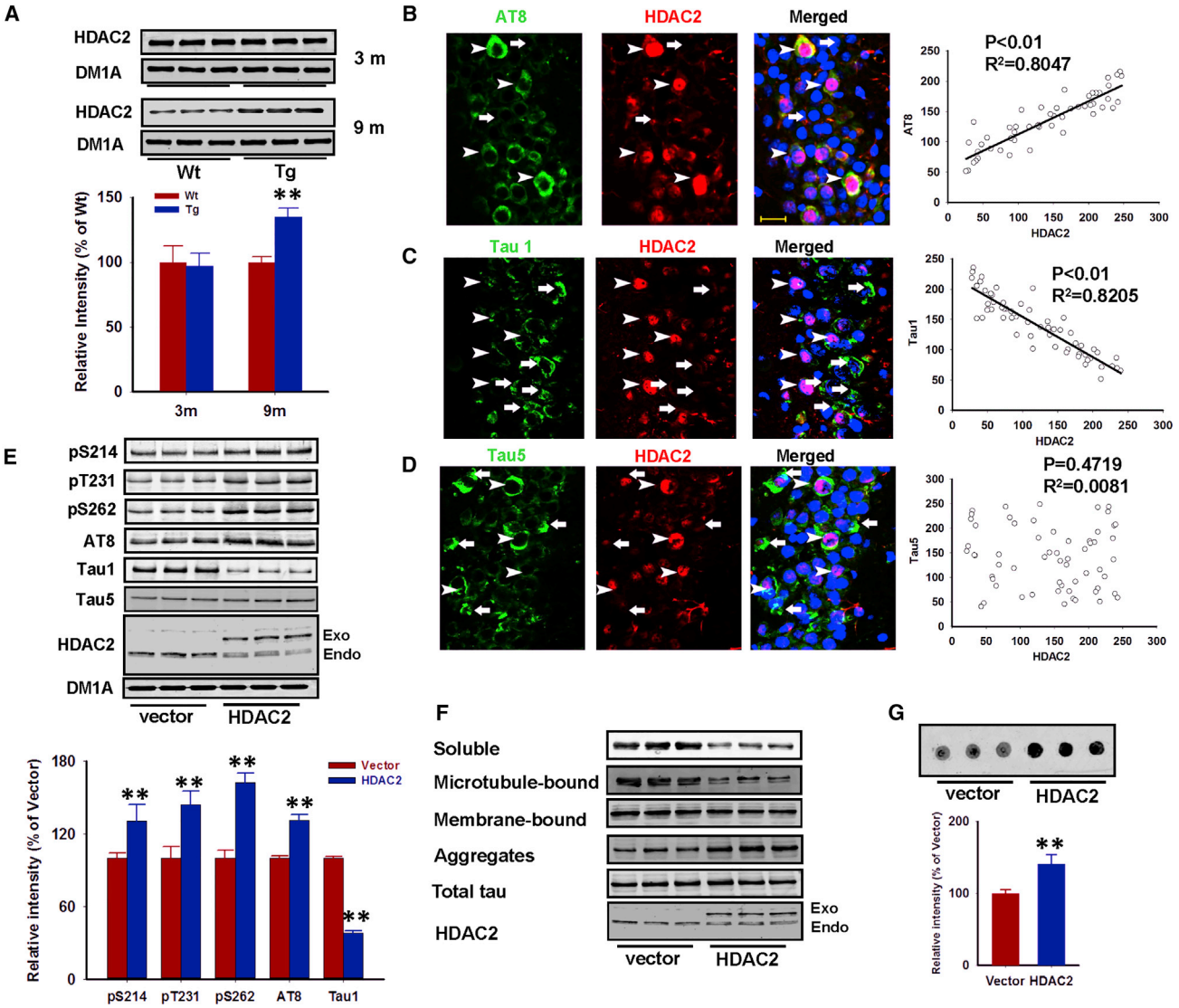

Figure 1. Overexpression of HDAC2 Induces Tauopathy and Dendritic Abnormalities

(A) Hippocampi homogenates were prepared from 3-month-old (3 m) and 12-month-old (12 m) 3xTg-AD mice (Tg) and normal littermates (Wt) and were evaluated via a western blot assay with an anti-HDAC2 antibody. Representative images and the results of a quantitative analysis are presented. **$p < 0.01$ (versus wild type; Student's t test; n = 3 independent experiments with six mice per group). (B–D) Three separate double immunofluorescence experiments were performed in hippocampal slices from 12-month-old 3xTg-AD mice using anti-AT8 (green) and anti-HDAC2 (red) antibodies (n = 52) (B), anti-Tau1 (green) and anti-HDAC2 (red) antibodies (n = 60) (C), or anti-Tau5 (green) and anti-HDAC2 (red) antibodies (n = 56) (D). Fluorescence intensities were measured using ImageJ software (NIH), and correlation analyses were performed with SigmaPlot software (Systat Software). Arrowheads indicate neurons with a high HDAC2 intensity; arrows indicate neurons with a low HDAC2 intensity. (E) Hippocampal neurons were cultured to 14 DIV and subsequently infected with HDAC2-expressing lentivirus (HDAC2) or vector control (vector). After 48 hr, the neurons were harvested and the cell lysates were used for western blot with the indicated antibodies for pS214, pT231, pS262, AT8, Tau1, Tau5, HDAC2, and DM1A. Representative blots and quantitative analyses are presented. **$p < 0.01$ (versus vector; Student's t test; n = 4 independent experiments). (F) HEK293 cells that stably expressed full-length human tau were transfected with pcDNA-HDAC2 or a control vector. Cell lysates were subsequently collected and dissociated into four fractions, including cytosolic soluble tau, microtubule-bound tau, membrane-bound tau, and SDS-soluble aggregated tau, for western blot using an anti-Tau-5 antibody (n = 3 independent experiments). (G) HEK293 cell lysates were also used for filter/trap analysis. The intensity of Tau5 immunoreactivity was measured, and quantitative analyses were performed. **$p < 0.01$ (versus vector; Student's t test; n = 3 independent experiments). Data are presented as mean ± SEM.

downregulated by 60%. In contrast, miR-19 was increased by 160%, whereas the other miRNAs remained unchanged (Figure 3D). Based on these findings, we focused our efforts on miR-101b. To verify the direct regulation of AMPK by miR-101b, we constructed a luciferase reporter that contained wild-type or mutant 3′ UTR segments of AMPK mRNA (Figure 3E). Following miR-10b expression, the

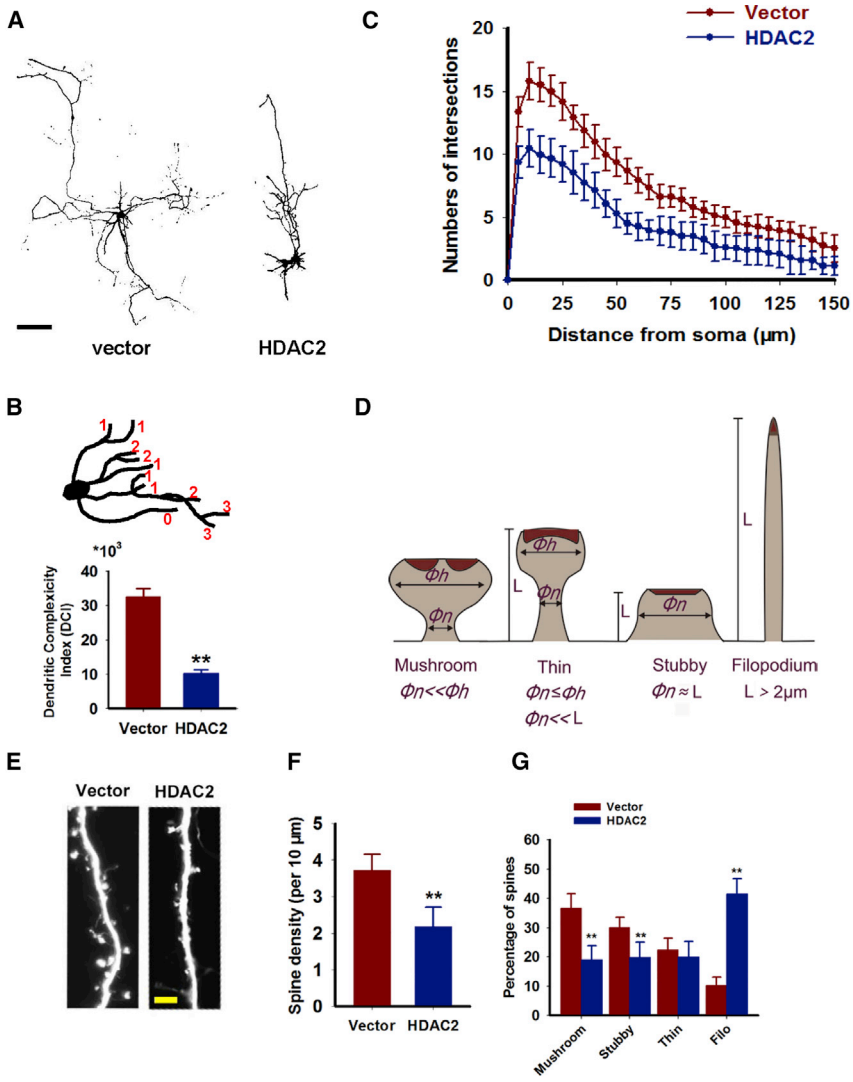

Figure 2. Overexpression of HDAC2 Induces Dendritic Abnormalities

(A–C) Mouse hippocampal neurons were cultured to DIV 7 and infected with lenti-HDAC2-GFP (HDAC2) or lenti-GFP (vector) for 72 hr. (A) Neurons were subsequently cultured to DIV 14, and confocal microscopy images were collected with an LSM710 laser confocal microscope. (B) DCIs were calculated as described in the Materials and Methods, and the branches were evaluated as labeled in the upper panel. **$p < 0.01$ (versus vector; Student's t test). (C) Sholl analysis was performed to measure the dendritic complexity ($n = 51–55$). (D–G) Hippocampal neurons were cultured and the dendritic spines were analyzed, with four spine types defined as indicated in (D). Φh, diameter of the head; Φn, diameter of the neck; L, spine height or side length. Red coloration indicates the postsynaptic density. (E) The spines were visualized using GFP that fused to the lentivirus. Quantitative analyses of the spine density (F) and the percentages of different spine types (G) were performed. **$p < 0.01$ (versus vector; Student's t test; $n = 32–34$). Data are presented as mean ± SEM.

wild-type reporter was strongly inhibited in contrast to that in the mutant (Figure 3F). The overexpression of miR-101b mimics and inhibitors (antagomirs) in primary neurons also modulated the endogenous AMPK protein (but not mRNA) levels (Figures 3G and 3H), which further confirms the post-transcriptional regulation of AMPK by miR-101b. Finally, we demonstrated that miR-101b upregulation restored AMPK protein levels by HDAC2 (Figures 3I and 3J). Thus, HDAC2-induced AMPK upregulation is mediated by miR-101b.

HDAC2 Negatively Regulates the Binding of HNF-4A to the miR-101b Promoter

To better understand how HDAC2 suppresses miR-101b expression, we measured miR-101 primary transcript levels (pri-miR-101b and pre-miR-101b) in the nucleus of primary hippocampal cultures. We determined that following HDAC2 overexpression, both pri-miR-101b and pre-miR-101b transcripts were substantially reduced (Figure 4A). Using online bioinformatic tools (MotifMap and TFBind), we identified 10 concentrated HNF-4A transcription factor binding motifs within the mouse miR-101 promoter (M01031 motif; Figures 4B and S7; Tables S1 and S2). To validate these predictions, we co-expressed the promoter region of miR-101b with HNF-4A into HEK293 cells. HNF-4A overexpression caused a 2.2-fold increase in miR-101b expression (luciferase intensity) compared with that in control cells (Figure 4C). In contrast, administration of a HNF-4A inhibitor (BI6015) or simultaneous HDAC2 overexpression significantly reduced luciferase intensity (Figure 4C). We also performed chromatin immunoprecipitation (ChIP) assays and identified a substantial decrease in HNF-4A binding to the endogenous miR-101 promoter following HDAC2 overexpression compared to that observed in control cells (Figure 4D).

Previous studies indicated that HNF-4A acetylation is required for its transcriptional activity.[18] Interestingly, the pan-acetylation levels of HNF-4A were substantially reduced (40% of the level identified in the vector controls) in HDAC2-overexpressing neurons (Figure 4E). According to a previous proteomics study, lysine 458 of HNF-4A is the only site that is regulated by acetylation.[19] We subsequently generated the K458A mutant of HNF-4A and determined that this mutant cannot induce miR-101b expression (luciferase intensity) to the same extent as wild-type HNF-4A (Figure 4C). Moreover, HDAC2 overexpression induced greater phosphorylation of HNF-4A at the Ser304 epitope (Figure 4F), which is phosphorylated by AMPK to inhibit its transcriptional activity.[20] Similar results were obtained from the hippocampus of 12-month-old 3xTg-AD mice

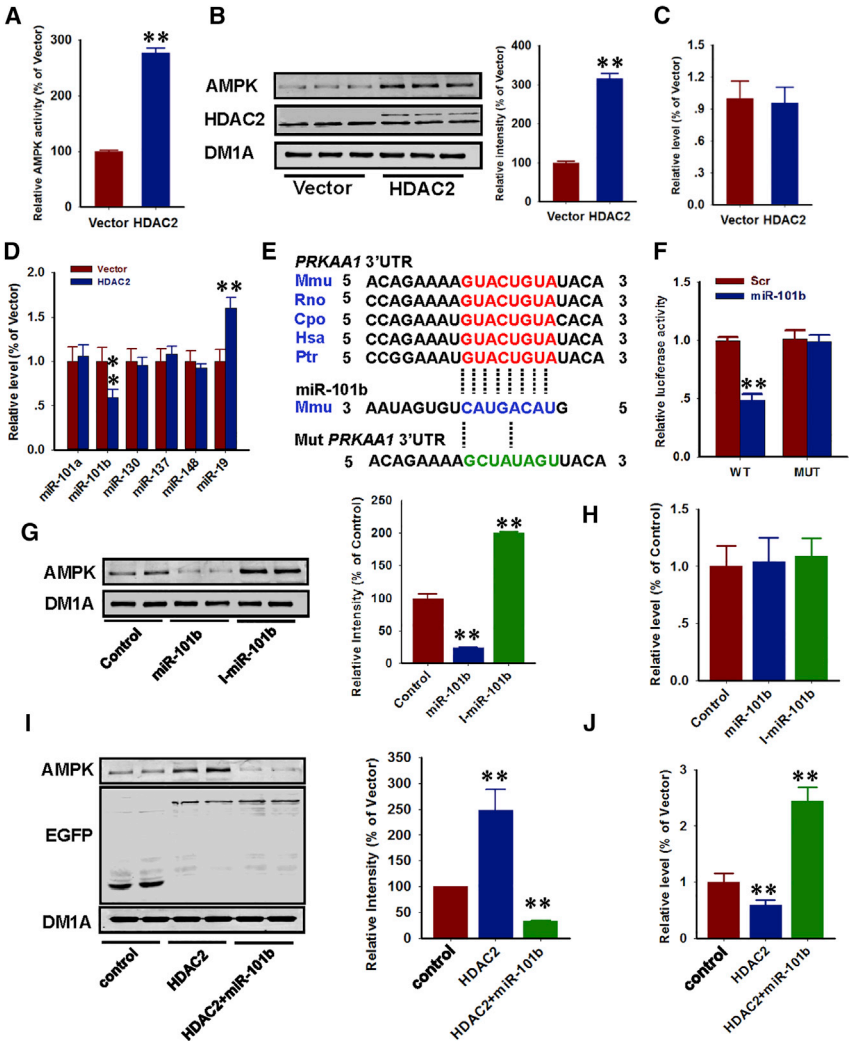

Figure 3. HDAC2 Induces AMPK Expression via Inhibition of miR-101b

(A–C) Cultured mouse hippocampal neurons were infected with lenti-HDAC2-GFP (HDAC2) or lenti-GFP (vector) for 72 hr, and the cell lysates were used to measure the AMPK activity via a commercial kit (A), as well as AMPK protein (B) and mRNA (C) levels. **$p < 0.01$ (versus vector; Student's t test; n = 4). (D) Total RNA was purified from infected mouse hippocampal neurons by the Tiangen miRNA extraction kit. qPCR was subsequently performed to determine the content of the listed miRNAs. **$p < 0.01$ (versus vector; Student's t test; n = 4). (E) Bioinformatic analysis indicates that the miR-101b binding site in the 3′ UTR of AMPK mRNA (*PRKAA1*) is conserved across mammals. (F) Both the wild-type and mutant 3′UTR of *PRKAA1* as indicated in (E) were constructed in the pSi-Check vector and co-transfected with miR-101b mimics (miR-101b) or scrambled control (Scr) into HEK293 cells; luciferase intensity was determined after 48 hr. **$p < 0.01$ (versus Scr; one-way ANOVA, Tukey's multiple comparisons test; n = 4). (G and H) Cultured mouse hippocampal neurons were transfected with miR-101b mimics (miR-101b) or miR-101b antagomirs (l-miR-101b), and the cell lysates were used to detect AMPK protein (G) and mRNA (H) levels. **$p < 0.01$ (versus control; one-way ANOVA, Tukey's multiple comparisons test; n = 4). (I and J) Cultured mouse hippocampal neurons were transfected with HDAC2 (HDAC2), HDAC2 plus miR-101b mimics (HDAC2+miR-101b), or eGFP plus antagomir control (control), and the cell lysates were used to detect the AMPK protein (I) and miR-101b (J) levels. **$p < 0.01$ (versus control; one-way ANOVA, Tukey's multiple comparisons test; n = 4). Data are presented as mean ± SEM.

(Figures 4G–4I). Therefore, the suppression of miR-101b by HDAC2 was further increased by activation of AMPK, which forms a strong regulatory feedback loop.

miR-101b Overexpression or AMPK Silencing Attenuates HDAC2-Induced Tauopathy and Dendritic Impairments

We subsequently investigated whether the restoration of miR-101b or AMPK could rescue the effects induced by HDAC2. We determined that overexpression of the miR-101b mimic or downregulation of AMPK using small interfering RNAs (siRNAs) reversed tau hyperphosphorylation following HDAC2 overexpression in neurons (Figures 5A–5G). miR-101b mimics or AMPK siRNAs also restored tau localization and aggregation (Figures 5H and 5I). Similar positive effects were identified on dendrites (Figures 6A–6C) and spines (Figures 6D–6F). Thus, rebuilding the miR-101b/AMPK pathway may rescue both AD-like pathologies induced by HDAC2.

miR-101b Overexpression or AMPK Silencing Rescues Memory Deficits in AD Mice

Finally, we investigated the miR-101b/AMPK pathway in 3xTg-AD mice, which were shown to have increased HDAC2 levels. We initially showed that the miR-101b and AMPK levels were affected in the hippocampus of 12-month-old 3xTg-AD mice but not 3-month-old 3xTg-AD mice (Figures 7A and 7B), which further suggests that this alteration is disease specific. Notably, the administration of miR-101b mimics or lentivirus-expressing AMPK siRNAs (si-AMPK) in 12-month-old 3xTg-AD mice improved their hippocampus-dependent memory in the Morris water maze (Figures 7C–7F). In fear conditioning tasks, we determined that the deficits in short-term and remote memory were substantially improved following the administration of miR-101b mimics or si-AMPK (Figures 7G–7I). As previously indicated, these treatments ameliorated tau phosphorylation (Figures 7J and 7K) and dendritic impairments in 3xTg-AD mice (Figures 7L–7N). Collectively, these findings demonstrate that a target-specific strategy to rebuild the miR-101b/AMPK pathway attenuates AD-like tauopathy and dendritic deficits in vivo.

DISCUSSION

HDAC2 is a class I histone deacetylase that predominantly localizes in the nucleus and plays important roles in neuronal development and

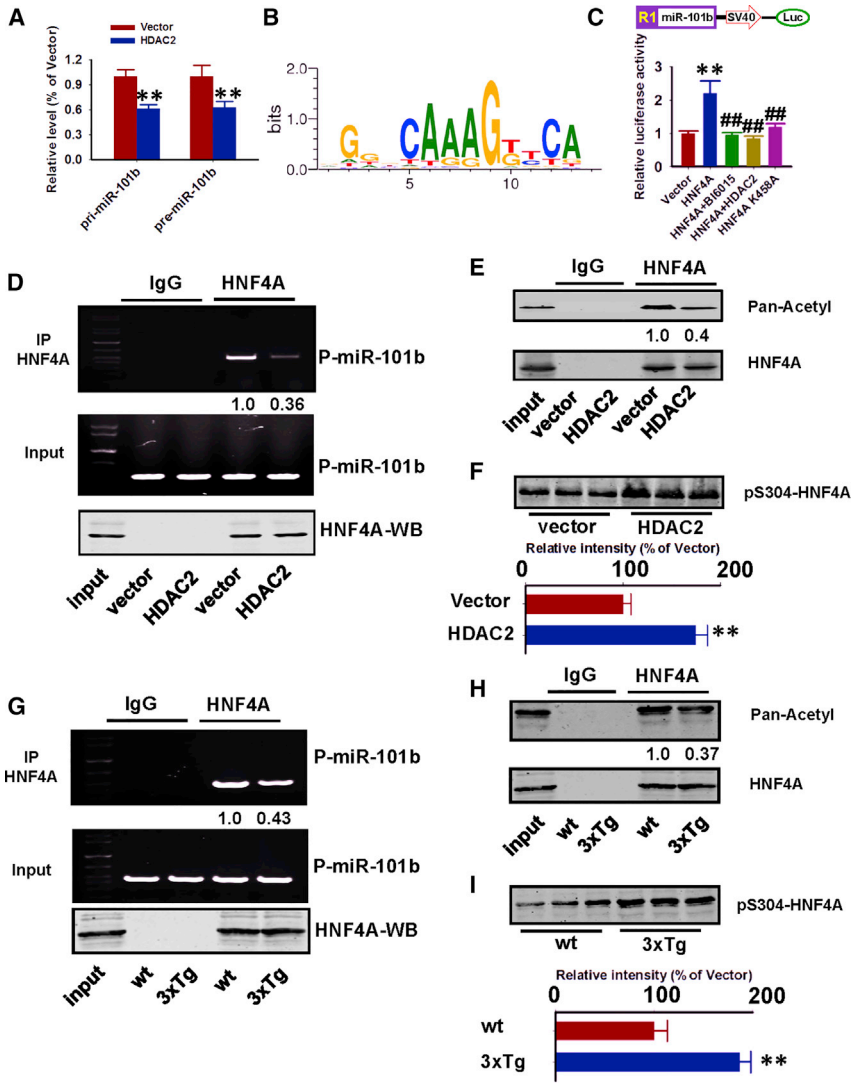

Figure 4. HDAC2 Suppresses miR-101b Transcription by Deacetylating HNF-4A

(A) Cultured mouse hippocampal neurons were transfected with HDAC2 (HDAC2) or the corresponding control vector (vector), and pri- and pre-miR-101b were detected by qPCR. **p < 0.01 (versus vector; one-way ANOVA, Tukey's multiple comparisons test; n = 4). (B) Diagram of the binding motif (M00134) of the HNF-4A transcription factor with the miR-101b promoter. (C) The promoter region of miR-101b was cloned into the pGL3 vector and was co-transfected with HNF-4A or its corresponding vector control. Luciferase activity was evaluated after 24 hr in transfected cells and cells treated with BI6015 (an HNF-4A inhibitor) or HNF-4A plus HDAC2. **p < 0.01, ##p < 0.01 (versus vector and HNF-4A, respectively; one-way ANOVA, Tukey's multiple comparisons test; n = 4). (D) Hippocampal neurons were transfected with HDAC2 or the corresponding control vector, and the cell lysates were used in a ChIP assay to examine the binding ability of HNF-4A with the miR-101b promoter following HDAC2 overexpression. Upper and middle panels, PCR; lower panel, western blot. HDAC2- or vector-control-infected neuronal lysates were immunoprecipitated with anti-HNF-4A antibody or IgG (n = 3 independent experiments). (E and F) Cell lysates were immunoprecipitated with anti-HNF-4A, and binding was detected with a pan-acetylation antibody (E). Cell lysates were analyzed via western blot to examine HNF-4A phosphorylation at Ser304 (F). **p < 0.01 (versus vector; Student's t test; n = 3 independent experiments). (G) A ChIP assay was performed in 12-month-old 3xTg-AD mice and wild-type control littermates (wt) using hippocampal homogenates. (H and I) Hippocampal homogenates were immunoprecipitated with anti-HNF-4A, and binding was detected with a pan-acetylation antibody (H). Homogenates were analyzed via western blot to examine HNF-4A phosphorylation at Ser304 (I). **p < 0.01 (versus wild type; Student's t test; n = 3 independent experiments). Data are presented as mean ± SEM.

adult synaptic plasticity.[21] In post-mortem brain samples from patients with non-familial AD, HDAC2 is elevated in the CA1 hippocampal area and in the entorhinal cortex, which represent two brain areas strongly affected by AD.[7] Furthermore, in a mouse model of AD, the application of HDAC inhibitors attenuates Aβ oligomer-induced drebrin loss from dendritic spines,[22] decreases Aβ levels, and improves learning and memory.[23] This evidence strongly suggests a critical role of HDAC2 in various aspects of AD pathogeneses, such as the amyloid precursor protein (APP) process, synaptic dysfunction, and memory impairment. The accumulation of HDAC2 also occurs at the beginning at Braak stages I/II, which are characterized by the accumulation of hyperphosphorylated tau protein in the brain, and correlates with cognitive decline. Here, we identified a positive correlation between HDAC2 expression and tau phosphorylation in the brains of AD-like mice. HDAC2 overexpression resulted in tau hyperphosphorylation and aggregation as well as dendritic impairments. Our data validate and extend the importance of epigenetic factors in the regulation of pathological changes associated with AD.

Tau undergoes multiple abnormal post-transcriptional modifications in AD, such as hyperphosphorylation or acetylation.[3] In this study, we determined that HDAC2 overexpression mainly affects tau phosphorylation. The screening of known tau kinases and phosphatases identified AMPK as a prominent effector. AMPK is a highly conserved serine/threonine protein kinase and metabolic sensor expressed in most mammalian cell types. It has been proposed that AMPK regulates neurodegeneration via the upregulation of BACE1 to increase the generation of both intracellular and extracellular Aβ levels[24] as well as via the direct phosphorylation of tau at Thr231 and Ser396/404.[25] Therefore, AMPK may represent a common denominator in neurodegenerative diseases and a promising target for

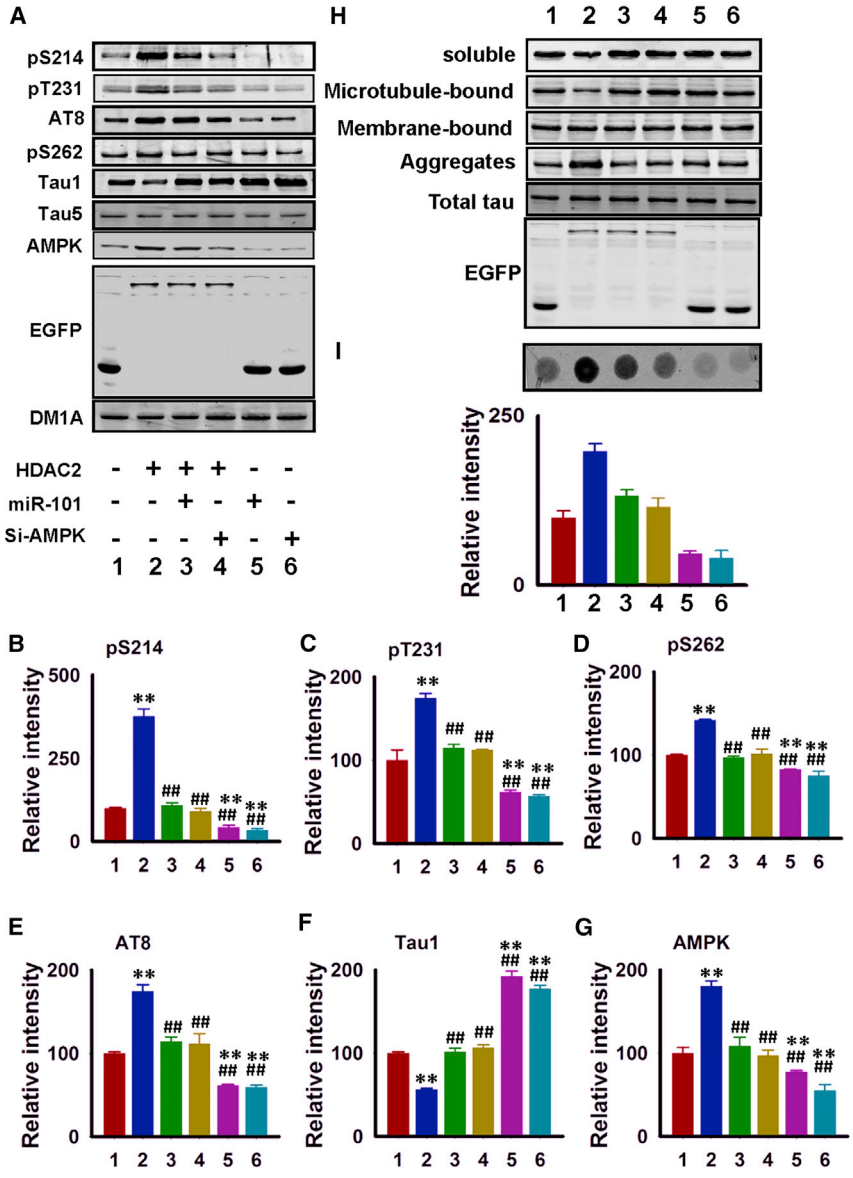

Figure 5. Administration of miR-101b Mimics or Silencing of AMPK Reduces Tauopathy

(A–G) Hippocampal neurons were transfected with control vectors (1), HDAC2 (2), HDAC2 plus miR-101b mimics (3), HDAC2 plus si-AMPK (4), miR-101b mimics alone (5), or si-AMPK alone (6), and cell lysates were prepared for western blot analysis as indicated. Representative blots are shown in (A), and quantitative analyses were performed for pS214 (B), pT231 (C), pS262 (D), AT8 (E), Tau 1 (F), and AMPK (G) (n = 4). (H) HEK293 cells stably transfected with human full-length tau were transfected with control vectors, HDAC2, HDAC2 plus miR-101b mimics, HDAC2 plus si-AMPK, miR-101b mimics alone, or si-AMPK alone. Cell lysates were collected and dissociated into four fractions, including cytosolic soluble tau, microtubule-bound tau, membrane-bound tau, and SDS-soluble aggregated tau, for western blot using an anti-Tau-5 antibody (n = 3). (I) HEK293 cells stably transfected with human full-length tau were transfected as described in (H). The cell lysates were subsequently subjected to filter/trap analysis. The intensity of Tau5 immunoreactivity was measured, and a quantitative analysis was performed (n = 3). Data are presented as mean ± SEM.

anti-AD drugs.[26] There are contradictory reports of AMPK activation in AD; however, new evidence suggests gender-specific effects of AMPK activation.[27] In addition, low levels of AMPK activation have been associated with improved cognition, whereas a higher degree of activation was linked to elevated catecholamine levels, induced neuronal apoptosis, and impaired cognition.[28] In a mouse model of AD, pharmacological activation of AMPK by the anti-diabetic drug metformin led to impaired learning and memory in male APP mice but was protective in female mice.[29] In our study, AMPK activity and expression were substantially increased following HDAC2 overexpression, which led to abnormal hyperphosphorylation and tau aggregation and the resultant mislocalization of tau to dendritic spines as well as decreased expression of the α-amino-3-hydroxy-5-methyl-4-isoxazolepropionic acid (AMPA) glutamate receptor, as previously reported.[4] AMPK silencing rescued both tauopathy and memory deficits in 3xTg-AD mice, which suggests a potential protective strategy for AD.

miRNAs are emerging as potential key players in the pathogenesis of AD.[30] Various miRNA alterations have been identified in patients with AD and in mouse models of AD,[31] and most alterations have been implicated in the regulation of key AD genes. Previous reports demonstrate that miR-101 is downregulated in the temporal and parietal cortices of patients with AD.[32] Notably, miR-101 is shown to downregulate APP and fibrillar Aβ in hippocampal neurons by directly targeting *APP*[33] or *RanBP9*, which encodes for the RanBP9 protein to enhance the proteolytic processing of APP and Aβ generation both in vivo and in vitro.[34] In the present study, we demonstrate that miR-101b directly targets the 3′ UTR of *AMPK* to post-transcriptionally regulate its protein levels. We further identified a physical binding of the HNF-4A transcription factor to the promoter region of miR-101b. While the binding of HNF-4A to the miR-101b promoter is under the control of acetylated HNF-4A,[18] HDAC2 overexpression reversed these effects.

Together, our findings not only identify a novel mechanism of HDAC2 action in the progression of AD but also indicate that this mechanism can restore the expression of miR-101b or AMPK and rescue AD mice from identified abnormalities (Figure 8). Moreover, these findings provide novel therapeutic candidates based on miRNAs and/or epigenetics.

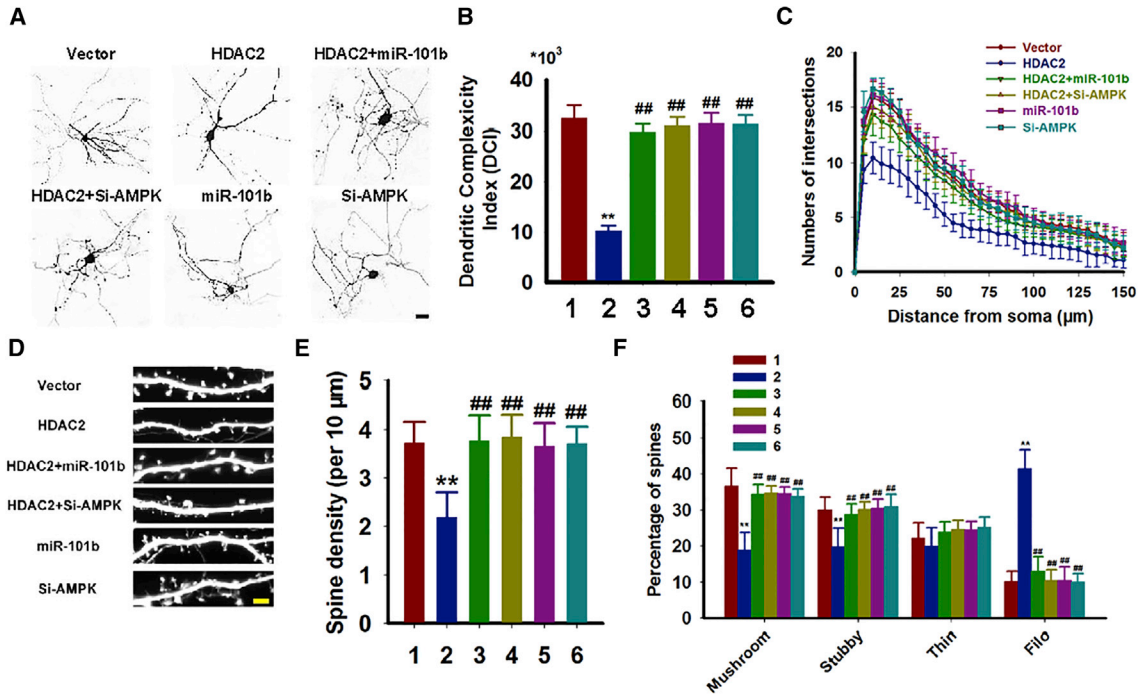

Figure 6. Administration of miR-101b Mimics or Silencing of AMPK Reduces Dendritic Abnormalities

(A–C) Mouse hippocampal neurons were cultured to DIV 7 and infected with control vectors (1), HDAC2 (2), HDAC2 plus miR-101b mimics (3), HDAC2 plus si-AMPK (4), miR-101b mimics alone (5), or si-AMPK alone (6) for 72 hr. (A) The neurons were subsequently cultured to DIV 14, and images were collected with an LSM710 laser confocal microscope. (B) DCIs were calculated as described in the Materials and Methods. $^{**}p < 0.01$, $^{\#\#}p < 0.01$ (versus vector and HDAC2, respectively). (C) Sholl analysis was performed to measure the dendritic complexity (n = 49–55). (D–F) Dendritic spines were visualized in cultured hippocampal neurons by the intensity of the GFP reporter fused to the lentivirus (D). Quantitative analyses of the spine density (E) and the percentages of different spine types (F) were performed. $^{**}p < 0.01$, $^{\#\#}p < 0.01$ (versus vector and HDAC2, respectively; n = 32–34). Data are presented as mean ± SEM.

MATERIALS AND METHODS

Antibodies and Reagents

All animal experiments were carried out according to the "Policies on the Use of Animals and Humans in Neuroscience Research" revised by the Society for Neuroscience in 1995 and approved by the animal ethnic committee of Huazhong University of Science and Technology.

All of the primary antibodies used in this study are listed in Table S3. The HDAC1 plasmid was a kind gift from Dr. Patrizia Casaccia at Mount Sinai School of Medicine. The cDNAs of HDAC2 and HDAC3 were obtained from in-house cDNA banks of mouse brain. All three cDNAs were constructed to the FUGW2.1 vector for viral packaging. Lipofectamine 2000 was purchased from Invitrogen. Cell culture media were from GIBCO. The short hairpin RNA (shRNA)-AMPK plasmid toward mouse AMPK (NM_001013367.3) was constructed to vector GV102 by Neuronbiotech. The primers used for AMPK were as follows: 5′-TCTGAGGGGCACCAAGAAAC-3′ (forward) and 5′-GTGGGTGTTGACGGAGAAGAG-3′ (reverse). The primers for miR-101a, miR-101b, miR-137, miR-19, miR-130, miR-148 detection, and miR-101b mimics and antagonimers were purchased from Ribobio. The HNF-4A (NM_008261.2) cDNA was cloned to the pcDNA3.0 vector by using the following primers: 5′-GGTAGGGGAGAATGCGACT-3′ (forward) and 5′-TAGGTTA CTCCCAGGTGCTC-3′ (reverse). The promoter sequence of miR-101b was cloned as shown in Figure S6.

Filter/Trap Assays for Tau Aggregates

Filter/trap assays were performed as described previously with minor modifications.[35] Cells were lysed in a buffer containing 0.5% Nonidet P-40, 1 mM EDTA, 50 mM Tris-HCl, pH 8.0, 120 mM NaCl, and a protease inhibitor mixture. After brief sonication, cell lysates were passed through a cellulose acetate membrane (0.2 μm; Bio-Rad) using a Bio-Dot Microfiltration Apparatus (Bio-Rad) and were washed for 15 min (three times) with 1% SDS followed by immunoblotting using Tau5 antibody. Quantitative dot-blot analyses were used to determine the level of tau aggregates.

ChIP Assay

The ChIP assay was performed as previously reported.[36] Briefly, cells were cross-linked in medium containing 1% formaldehyde for 10 min at room temperature. Cells were then lysed for ChIP in buffer containing 50 mM Tris-HCl, pH 8.1, 1% SDS, 10 mM EDTA, and Complete Protease Inhibitor Cocktail (Roche), then sonified to obtain 200- to 1,000-bp DNA fragments. ChIP was performed according to the ChIP Assay Kit (Millipore) protocol. Primers for the miR-101b promoter

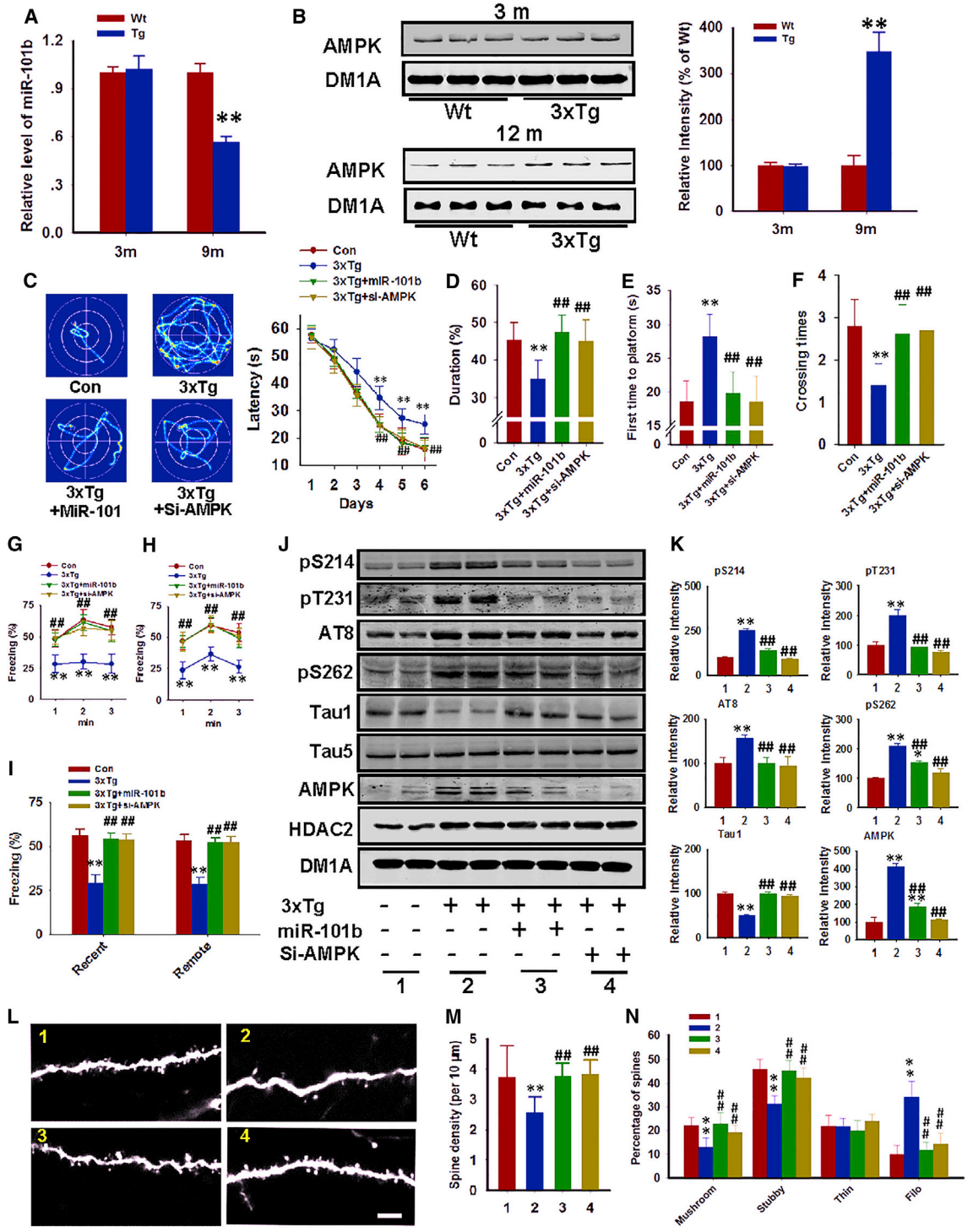

Figure 7. miR-101b Overexpression or AMPK Silencing Rescues Memory Deficits in AD Mice

(A and B) Hippocampi homogenates were prepared from 3-month-old (3 m) and 12-month-old (12 m) 3xTg-AD mice (Tg) and wild-type (Wt) littermates. miR-101b mRNA (A) and AMPK protein (B) levels were analyzed. **$p < 0.01$ (versus wild type; Student's t test; n = 4). (C) miR-101b mimics (3xTg-AD+miR-101b) or lentivirus-packed AMPK-siRNA (3xTg-AD+si-AMPK) were injected into the hippocampus of 12-month-old 3xTg-AD mice, and their memory functions were analyzed with the Morris water maze. Representative traces and latencies to the platform were recorded. $^{\#\#}p < 0.01$ (versus wild type and 3xTg-AD, respectively; only one symbol is labeled because of space limitations; two-way ANOVA, Bonferroni multiple comparisons test; n = 12). Animals treated with miR-101b mimics and AMPK-siRNA virus both exhibit reduced

(legend continued on next page)

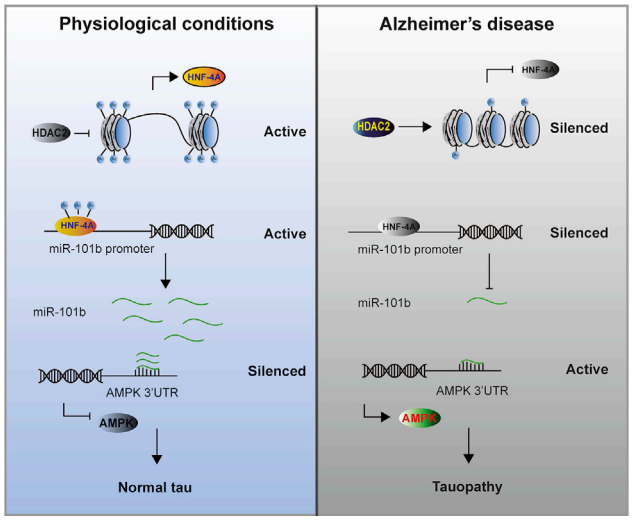

Figure 8. Diagram of the Current Study

In the AD brain, HDAC2 is upregulated and induces the deacetylation of the HNF-4A transcription factor, which leads to the inhibition of HNF-4A and the suppression of miR-101b expression. The loss of miR-101b induces AMPK overexpression and ultimately results in tauopathy. Data are presented as mean ± SEM.

region were as follows: 5′-TGCTGGCATCCTTTTTCCTT-3′ (forward) and 5′-CTACCTGCCCCTCCCACTT-3′ (reverse).

Immunofluorescence and Confocal Microscopy

A total of four 3xTg-AD [Tg(APPSwe,tauP301L)1Lfa, MMRRC stock no. 34830-JAX][37] mice were euthanized at 12 months by an overdose of chloral hydrate (1 g/kg) and were perfused with 100 mL 0.9% NaCl followed by 400 mL phosphate buffer containing 4% paraformaldehyde through the aorta. Two hours later, the brains were rapidly dissociated and post-fixed in perfusate overnight and then cut into sections (15–20 μm) with a vibratome (S100, TPI; Leica). Mouse brain sections were collected consecutively in PBS for immunofluorescence staining. Free-floating sections were incubated in BSA to block non-specific sites for 30 min at 25°C. Sections were then incubated overnight at 4°C with primary antibodies and rabbit HDAC2 antibody for 24 hr. Sections were washed with PBS and were subsequently incubated with mouse monoclonal Tau1, Tau5, or AT8 for another 24 hr. Sections were then washed with PBS for 30 min and were subsequently incubated with secondary antibodies Alexa Fluor 488 (donkey anti-mouse) or Alexa Fluor 546 (goat anti-rabbit) for 1 hr at 37°C. The hippocampal region was imaged using a laser confocal microscope (LSM780; Carl Zeiss).[38]

Morris Water Maze

As described in our previous studies,[39] spatial learning and memory were assessed by the Morris water maze test. For spatial learning, the mice were trained to find a hidden platform in the water maze for 6 consecutive days, four trials per day (with a 1-min interval) from 14:00 to 20:00 pm. Each trial began when the mouse started from one of the four quadrants facing the wall of the pool and ended when the animal climbed on the platform. If the mouse did not locate the platform within 60 s, the animal was guided to the platform. The swimming path and the time used to locate the platform (latency) were recorded by a video camera fixed to the ceiling of the room, 1.5 m from the water surface. On day 7, mice were tested on the time taken to find the hidden platform (escape latency), and the swimming path from the first quadrant by the camera was connected to a digital-tracking device attached to an IBM computer. Spatial memory was tested 2 days after training (day 9). The platform was removed and we recorded the percentage of time spent and total distances in the target quadrant and the number of platform quadrant crosses.

Contextual Fear Conditioning

During the training phase of the fear conditioning, the animals were placed in the conditioning chamber for 3 min and then were subjected to 180-s unsignaled footshocks (one shock at the first 60 s, three shocks at the second 60 s, and eight shocks at the third 60 s; 0.5 mA, 2-s duration, and 1 min apart). After the last shock, animals were kept in the chamber for another 60 s and were then returned to their home cages. During the testing phase, the animals were placed back into the conditioning chamber for 180 s. At the end of each session, animals were returned to their home cages and the chambers were cleaned with 70% ethanol. The conditioning chamber had a plexiglas front and gray side and back walls (175-mm wide × 165-mm deep × 300-mm high), and the chamber floors consisted of 26 stainless-steel rods (2-mm diameter) placed 5 mm apart. The rods were connected to a shock generator via a cable harness. All experiments were conducted using a video tracking system to measure the activity and freezing behavior of the animals. Freezing was defined as a complete absence of movement, and the duration of the freezing

latencies compared with the vehicle-treated 3xTg-AD mice. (D–F) On the ninth day of the Morris water maze test, the platform was removed to perform the probe test. The total time spent in the target quadrant (D), the first time to reach the platform (E), and the crossing times to the platform region (F) were analyzed. $^{**}p < 0.01$, $^{\#\#}p < 0.01$ (versus wild type and 3xTg-AD, respectively; one-way ANOVA, Newman-Keuls multiple comparisons test; n = 12). (G–I) Mice were also subjected to an analysis of contextual fear memory. A retrieval test of the freezing response measured at 24 hr after fear training (recent memory) (G) and at 28 days after fear training (remote memory) (H) and quantitative analyses of the average freezing response over the 3-min session (I) were performed. $^{**}p < 0.01$, $^{\#\#}p < 0.01$ (versus wild type and 3xTg-AD, respectively; two-way ANOVA, Bonferroni multiple comparisons test; n = 12). (J and K) Mouse hippocampi were extracted, and tau protein phosphorylation was analyzed. Representative images are shown in (J), and quantitative analyses were performed in (K). $^{**}p < 0.01$, $^{\#\#}p < 0.01$ (versus groups 1 and 2, respectively; two-way ANOVA, Bonferroni multiple comparisons test. n = 4). Groups are as follows: group 1, wild-type mice; group 2, 3xTg-AD mice; group 3, 3xTg-AD mice plus miR-101b mimics; and group 4, 3xTg-AD mice plus si-AMPK. (L–N) Brain slices were collected from the mice treated as previously described. The dendritic spines were visualized by a GFP-expressing virus (L), which was co-injected with miR-101b mimics, lenti-si-AMPK, or control. Quantitative analyses of the spine density (M) and the percentage of different spine types (N) were performed in 28 neurons from three mice per group. $^{**}p < 0.01$, $^{\#\#}p < 0.01$ (versus groups 1 and 2, respectively; two-way ANOVA, Bonferroni multiple comparisons test; n = 4). Data are presented as mean ± SEM.

response was scored at 1 s after the sustained freezing behavior. For each testing session, freezing (in percentages) was then averaged among animals within the same group.[40]

Primary Hippocampal Neuron Culture

Cultures of dissociated hippocampal neurons were prepared from embryonic E18 mice as previously described.[41,42] The hippocampi of embryos were dissected and trypsinized by TrypLE Express (Invitrogen) for 15 min at 37°C. Dissociated neurons were plated onto poly(D-lysine)-coated (Sigma) coverslips in a 12-well plate or tissue culture dish covered with a glass bottom (WPI) at a higher density (400–600 neurons/mm^2) for western blotting and a lower density (100–200 neurons/mm^2) for immunofluorescence. Neurons usually attached to the substrate after they grew in the plating medium (DMEM/F12 with 10% fetal bovine serum [FBS] and 100 U/mL penicillin/streptomycin) for 2–4 hr. Neurobasal medium (Invitrogen) supplemented with 2% B-27 (Invitrogen) was then replaced after attachment every 3 days. For virus infection, cultures were infected with lentivirus (purchased from Neuron Biotech). The titer of the virus reached 5×10^8 IU/mL and 10 μL virus was added to 290 μL condition medium per well in a six-well plate expressing HDAC2-EGFP, HDAC1-EGFP, HDAC3-EGFP, FUGW2.1 vector alone, or lenti-si-AMPK or lenti-scrambled si-AMPK at day in vitro (DIV) 7 for 72 hr. Infected neurons were cultured until DIV 14 for further biochemical, morphological, and imaging analyses. The dendritic complexity index was calculated for each neuron, as reported previously: DCI = [(sum of branch tip orders + number of branch tips)(total arbor length)/(number of primary dendrites)].[43] The Sholl analysis was used to determine the complexity of dendrites, as previously described.[44] The dendritic spines were measured according to a previously reported method in two segments of 20 μm each (90–110 μm and 190–210 μm from the soma) on one of the main branches.[45]

Real-Time PCR

Total RNA from cells was extracted with TRIzol reagent (Invitrogen), and 1 μg RNA was reverse transcribed. qRT-PCR was performed on an ABI StepOne Plus system (Applied Biosystems) using SYBR Green Premix Ex Taq (Takara). MicroRNA was extracted using a miRNA isolation kit (Tiangen). Reactions were prepared in a total volume of 10 μL containing the following: 0.5 μL cDNA (100 ng/μL), 1 μL of each 2-μM primer (300 mM each), 5 μL SYBR Green, and 2.5 μL RNase/DNase-free sterile water. Blank controls were run in triplicate for each master mix. Cycle conditions were set as follows: initial template denaturation at 95°C for 1 min, followed by 40 cycles of denaturation at 95°C for 5 s, combined primer annealing at 60°C for 30 s, and elongation at 72°C for 30 s. This cycle was followed by a melting curve analysis, ranging from 60°C to 95°C, with temperature increases by steps of 0.5°C every 10 s. Primers for miRNA detection were purchased from GeneCopoeia. MicroRNA was extracted using a miRNA isolation kit (Tiangen).

Western Blotting

Cells were rinsed twice in PBS at pH 7.5 and lysed with buffer containing 50 mM Tris-HCl, pH 8.0, 150 mM NaCl, 1% NP-40, 0.5% sodium deoxycholate, 0.1% SDS, 0.02% NaN_3, 100 μg/mL PMSF, and 10 μg/mL each of the protease inhibitors (leupeptin, aprotinin, and pepstatin A), followed by boiling for 5–6 min and then sonication for 5 s on ice. Cell lysates were then centrifuged at 12,000 × *g* for 5 min at 4°C; aliquots of supernatants were added to one-third volume of 4× sample buffer, 10% beta-mercaptoethanol (ME), and 0.05% bromophenol blue and then stored at −20°C or used immediately. Protein concentration was quantitated using the BCA Protein Assay Reagent (Pierce).[42,46]

Equal amounts of protein were separated by SDS-PAGE (10% gel) and transferred to nitrocellulose membranes. The membranes were blocked with 5% non-fat milk dissolved in PBS (50 mM Tris-HCl, pH 7.6, 150 mM NaCl) for 30 min to 1 hr and were probed with primary antibodies overnight at 4°C. Then the blots were incubated with goat anti-mouse or anti-rabbit conjugated to IRdye 800 (1:15,000; Rockland Immunochemicals) for 1 hr at 25°C. The protein bands were visualized and quantified by the Odyssey infrared imaging system (LI-COR). Levels of phosphorylated protein tau were normalized against the total protein tau; protein levels of PKA, GSK-3β, PP2Ac, and cdk5 were normalized against α-tubulin (DM1A); and the amount of protein was expressed as the relative level of the sum optical density against controls.

The tau fractioning analysis was performed as reported previously.[12] HEK293/tau cells were harvested 48 hr after transfection and lysed in breaking buffer with 0.25 M sucrose/10 mM HEPES, pH 7.2/1 mM $MgOAc_2$/protease inhibitors mixture. The cytosol fraction was prepared from the post-nuclear supernatant by ultracentrifugation for 1 hr at 190,000 × *g*. The resulting membrane pellet was resuspended and incubated on ice for 30 min with 5 μM nocodazole, followed by ultracentrifugation for 1 hr at 190,000 × *g* to produce post-nocodazole supernatants that contain the microtobule-bound tau. The generated pellets containing both membrane-associated and aggregated tau were further extracted using 100 mM sodium carbonate buffer, pH 11.5, at 4°C for another 30 min. The post-Na_2CO_3 pellets were prepared by ultracentrifugation at 190,000 × *g* for 1 hr and washed with 1% SDS to produce a fraction containing tau aggregates. Aliquots containing equal amounts of protein were analyzed by SDS-PAGE/western blotting for tau using Tau5. Western blotting results were quantified by densitometry to determine the tau level in each fraction.

Statistical Analysis

Data are presented as means ± SEM. All statistical tests were performed with GraphPad Prism software (version 5) as previously reported.[47] Statistical analysis was performed by using the Student's t test or ANOVA, followed by tests as specified in the figure legends, respectively. The statistical significance of experiments involving two experimental conditions was assessed by the unpaired Student's t test (two-sided), whereas that of experiments involving three or more experimental conditions was assessed by one-way ANOVA followed by the Tukey, Newman-Keuls, or Bonferroni post hoc test. Correlations were assessed by linear regression and Spearman's correlation. Null hypotheses were rejected at $p < 0.05$.

SUPPLEMENTAL INFORMATION

Supplemental Information includes seven figures and three tables can be found with this article online at http://dx.doi.org/10.1016/j.ymthe.2017.01.018.

AUTHOR CONTRIBUTIONS

L.-Q.Z. initiated, designed, and directed this study. D.L., H.T., N.W., X.-Y.L., Y.-F.Z., X.W., D.-Q.W., and M.-F.D. performed the experiments. J.-G.C., Y.L., P.F., and S.S.H. provided some comments. D.L., S.S.H., and L.-Q.Z. wrote the manuscript. All authors read and approved the final manuscript.

CONFLICTS OF INTEREST

All authors declare that they have no conflicts of interest.

ACKNOWLEDGMENTS

This study is partially supported by the National Natural Science Foundation of China (grants 31571039, 91632114, 81400899, 81361120245, 81400897, and 81400963), the 2014 Top-Notch Young Talents Program of China, the Program of Outstanding Youth of Hubei Province, China (grant 2014CFA017), the Academic Frontier Youth Team of Huazhong University of Science and Technology (to L.-Q.Z.), and the Program for Changjiang Scholars and Innovative Research Team in University (grant IRT13016).

REFERENCES

1. Fargo, K.N., Aisen, P., Albert, M., Au, R., Corrada, M.M., DeKosky, S., Drachman, D., Fillit, H., Gitlin, L., Haas, M., et al.; Alzheimer's Association National Plan Milestone Workgroup (2014). 2014 Report on the milestones for the US national plan to address Alzheimer's disease. Alzheimers Dement *10*, S430–S452.
2. Hu, W., Zhang, X., Tung, Y.C., Xie, S., Liu, F., and Iqbal, K. (2016). Hyperphosphorylation determines both the spread and the morphology of tau pathology. Alzheimers Dement *12*, 1066–1077.
3. Holtzman, D.M., Carrillo, M.C., Hendrix, J.A., Bain, L.J., Catafau, A.M., Gault, L.M., Goedert, M., Mandelkow, E., Mandelkow, E.M., Miller, D.S., et al. (2016). Tau: from research to clinical development. Alzheimers Dement *12*, 1033–1039.
4. Hoover, B.R., Reed, M.N., Su, J., Penrod, R.D., Kotilinek, L.A., Grant, M.K., Pitstick, R., Carlson, G.A., Lanier, L.M., Yuan, L.L., et al. (2010). Tau mislocalization to dendritic spines mediates synaptic dysfunction independently of neurodegeneration. Neuron *68*, 1067–1081.
5. Adwan, L., and Zawia, N.H. (2013). Epigenetics: a novel therapeutic approach for the treatment of Alzheimer's disease. Pharmacol. Ther. *139*, 41–50.
6. Gräff, J., Kim, D., Dobbin, M.M., and Tsai, L.H. (2011). Epigenetic regulation of gene expression in physiological and pathological brain processes. Physiol. Rev. *91*, 603–649.
7. Gräff, J., Rei, D., Guan, J.S., Wang, W.Y., Seo, J., Hennig, K.M., Nieland, T.J., Fass, D.M., Kao, P.F., Kahn, M., et al. (2012). An epigenetic blockade of cognitive functions in the neurodegenerating brain. Nature *483*, 222–226.
8. Guan, J.S., Haggarty, S.J., Giacometti, E., Dannenberg, J.H., Joseph, N., Gao, J., Nieland, T.J., Zhou, Y., Wang, X., Mazitschek, R., et al. (2009). HDAC2 negatively regulates memory formation and synaptic plasticity. Nature *459*, 55–60.
9. Holtzman, D.M., Morris, J.C., and Goate, A.M. (2011). Alzheimer's disease: the challenge of the second century. Sci. Transl. Med. *3*, 77sr1.
10. Jankowsky, J.L., Fadale, D.J., Anderson, J., Xu, G.M., Gonzales, V., Jenkins, N.A., Copeland, N.G., Lee, M.K., Younkin, L.H., Wagner, S.L., et al. (2004). Mutant presenilins specifically elevate the levels of the 42 residue beta-amyloid peptide in vivo: evidence for augmentation of a 42-specific gamma secretase. Hum. Mol. Genet. *13*, 159–170.
11. Alonso, A.D., Beharry, C., Corbo, C.P., and Cohen, L.S. (2016). Molecular mechanism of prion-like tau-induced neurodegeneration. Alzheimers Dement *12*, 1090–1097.
12. Zhang, X., Zhang, Y.W., Liu, S., Bulloj, A., Tong, G.G., Zhang, Z., Liao, F.F., and Xu, H. (2006). Tumor suppressor PTEN affects tau phosphorylation: deficiency in the phosphatase activity of PTEN increases aggregation of an FTDP-17 mutant Tau. Mol. Neurodegener. *1*, 7.
13. Zhang, X., Li, F., Bulloj, A., Zhang, Y.W., Tong, G., Zhang, Z., Liao, F.F., and Xu, H. (2006). Tumor-suppressor PTEN affects tau phosphorylation, aggregation, and binding to microtubules. FASEB J. *20*, 1272–1274.
14. Xiong, Y.S., Liu, F.F., Liu, D., Huang, H.Z., Wei, N., Tan, L., Chen, J.G., Man, H.Y., Gong, C.X., Lu, Y., et al. (2015). Opposite effects of two estrogen receptors on tau phosphorylation through disparate effects on the miR-218/PTPA pathway. Aging Cell *14*, 867–877.
15. Chang, E., and Kuret, J. (2008). Detection and quantification of tau aggregation using a membrane filter assay. Anal. Biochem. *373*, 330–336.
16. Mandelkow, E.M., and Mandelkow, E. (2012). Biochemistry and cell biology of tau protein in neurofibrillary degeneration. Cold Spring Harb. Perspect. Med. *2*, a006247.
17. Williams, A.E. (2008). Functional aspects of animal microRNAs. Cell. Mol. Life Sci. *65*, 545–562.
18. Soutoglou, E., Katrakili, N., and Talianidis, I. (2000). Acetylation regulates transcription factor activity at multiple levels. Mol. Cell *5*, 745–751.
19. Lundby, A., Lage, K., Weinert, B.T., Bekker-Jensen, D.B., Secher, A., Skovgaard, T., Kelstrup, C.D., Dmytriyev, A., Choudhary, C., Lundby, C., et al. (2012). Proteomic analysis of lysine acetylation sites in rat tissues reveals organ specificity and subcellular patterns. Cell Rep. *2*, 419–431.
20. Hong, Y.H., Varanasi, U.S., Yang, W., and Leff, T. (2003). AMP-activated protein kinase regulates HNF4alpha transcriptional activity by inhibiting dimer formation and decreasing protein stability. J. Biol. Chem. *278*, 27495–27501.
21. Montgomery, R.L., Hsieh, J., Barbosa, A.C., Richardson, J.A., and Olson, E.N. (2009). Histone deacetylases 1 and 2 control the progression of neural precursors to neurons during brain development. Proc. Natl. Acad. Sci. USA *106*, 7876–7881.
22. Ishizuka, Y., Shimizu, H., Takagi, E., Kato, M., Yamagata, H., Mikuni, M., and Shirao, T. (2014). Histone deacetylase mediates the decrease in drebrin cluster density induced by amyloid beta oligomers. Neurochem. Int. *76*, 114–121.
23. Sung, Y.M., Lee, T., Yoon, H., DiBattista, A.M., Song, J.M., Sohn, Y., Moffat, E.I., Turner, R.S., Jung, M., Kim, J., et al. (2013). Mercaptoacetamide-based class II HDAC inhibitor lowers Aβ levels and improves learning and memory in a mouse model of Alzheimer's disease. Exp. Neurol. *239*, 192–201.
24. Chen, Y., Zhou, K., Wang, R., Liu, Y., Kwak, Y.D., Ma, T., Thompson, R.C., Zhao, Y., Smith, L., Gasparini, L., et al. (2009). Antidiabetic drug metformin (GlucophageR) increases biogenesis of Alzheimer's amyloid peptides via up-regulating BACE1 transcription. Proc. Natl. Acad. Sci. USA *106*, 3907–3912.
25. Vingtdeux, V., Davies, P., Dickson, D.W., and Marambaud, P. (2011). AMPK is abnormally activated in tangle- and pre-tangle-bearing neurons in Alzheimer's disease and other tauopathies. Acta Neuropathol. *121*, 337–349.
26. Cai, Z., Yan, L.J., Li, K., Quazi, S.H., and Zhao, B. (2012). Roles of AMP-activated protein kinase in Alzheimer's disease. Neuromolecular Med. *14*, 1–14.
27. Vázquez-Manrique, R.P., Farina, F., Cambon, K., Dolores Sequedo, M., Parker, A.J., Millán, J.M., Weiss, A., Déglon, N., and Neri, C. (2016). AMPK activation protects from neuronal dysfunction and vulnerability across nematode, cellular and mouse models of Huntington's disease. Hum. Mol. Genet. *25*, 1043–1058.
28. Salminen, A., Kaarniranta, K., Haapasalo, A., Soininen, H., and Hiltunen, M. (2011). AMP-activated protein kinase: a potential player in Alzheimer's disease. J. Neurochem. *118*, 460–474.
29. DiTacchio, K.A., Heinemann, S.F., and Dziewczapolski, G. (2015). Metformin treatment alters memory function in a mouse model of Alzheimer's disease. J. Alzheimers Dis. *44*, 43–48.
30. Delay, C., Mandemakers, W., and Hébert, S.S. (2012). MicroRNAs in Alzheimer's disease. Neurobiol. Dis. *46*, 285–290.
31. Delay, C., and Hébert, S.S. (2011). MicroRNAs and Alzheimer's disease mouse models: current insights and future research avenues. Int. J. Alzheimers Dis. *2011*, 894938.

32. Hébert, S.S., Horré, K., Nicolaï, L., Papadopoulou, A.S., Mandemakers, W., Silahtaroglu, A.N., Kauppinen, S., Delacourte, A., and De Strooper, B. (2008). Loss of microRNA cluster miR-29a/b-1 in sporadic Alzheimer's disease correlates with increased BACE1/beta-secretase expression. Proc. Natl. Acad. Sci. USA *105*, 6415–6420.

33. Vilardo, E., Barbato, C., Ciotti, M., Cogoni, C., and Ruberti, F. (2010). MicroRNA-101 regulates amyloid precursor protein expression in hippocampal neurons. J. Biol. Chem. *285*, 18344–18351.

34. Barbato, C., Pezzola, S., Caggiano, C., Antonelli, M., Frisone, P., Ciotti, M.T., and Ruberti, F. (2014). A lentiviral sponge for miR-101 regulates RanBP9 expression and amyloid precursor protein metabolism in hippocampal neurons. Front. Cell. Neurosci. *8*, 37.

35. Dou, F., Netzer, W.J., Tanemura, K., Li, F., Hartl, F.U., Takashima, A., Gouras, G.K., Greengard, P., and Xu, H. (2003). Chaperones increase association of tau protein with microtubules. Proc. Natl. Acad. Sci. USA *100*, 721–726.

36. Lodrini, M., Oehme, I., Schroeder, C., Milde, T., Schier, M.C., Kopp-Schneider, A., Schulte, J.H., Fischer, M., De Preter, K., Pattyn, F., et al. (2013). MYCN and HDAC2 cooperate to repress miR-183 signaling in neuroblastoma. Nucleic Acids Res. *41*, 6018–6033.

37. Oddo, S., Caccamo, A., Shepherd, J.D., Murphy, M.P., Golde, T.E., Kayed, R., Metherate, R., Mattson, M.P., Akbari, Y., and LaFerla, F.M. (2003). Triple-transgenic model of Alzheimer's disease with plaques and tangles: intracellular Abeta and synaptic dysfunction. Neuron *39*, 409–421.

38. Chen, L.M., Xiong, Y.S., Kong, F.L., Qu, M., Wang, Q., Chen, X.Q., Wang, J.Z., and Zhu, L.Q. (2012). Neuroglobin attenuates Alzheimer-like tau hyperphosphorylation by activating Akt signaling. J. Neurochem. *120*, 157–164.

39. Peng, C.X., Hu, J., Liu, D., Hong, X.P., Wu, Y.Y., Zhu, L.Q., and Wang, J.Z. (2013). Disease-modified glycogen synthase kinase-3β intervention by melatonin arrests the pathology and memory deficits in an Alzheimer's animal model. Neurobiol. Aging *34*, 1555–1563.

40. Kitamura, T., Saitoh, Y., Takashima, N., Murayama, A., Niibori, Y., Ageta, H., Sekiguchi, M., Sugiyama, H., and Inokuchi, K. (2009). Adult neurogenesis modulates the hippocampus-dependent period of associative fear memory. Cell *139*, 814–827.

41. Kaech, S., and Banker, G. (2006). Culturing hippocampal neurons. Nat. Protoc. *1*, 2406–2415.

42. Liu, D., Wei, N., Man, H.Y., Lu, Y., Zhu, L.Q., and Wang, J.Z. (2015). The MT2 receptor stimulates axonogenesis and enhances synaptic transmission by activating Akt signaling. Cell Death Differ. *22*, 583–596.

43. Lom, B., and Cohen-Cory, S. (1999). Brain-derived neurotrophic factor differentially regulates retinal ganglion cell dendritic and axonal arborization in vivo. J. Neurosci. *19*, 9928–9938.

44. Shin, E., Kashiwagi, Y., Kuriu, T., Iwasaki, H., Tanaka, T., Koizumi, H., Gleeson, J.G., and Okabe, S. (2013). Doublecortin-like kinase enhances dendritic remodelling and negatively regulates synapse maturation. Nat. Commun. *4*, 1440.

45. Bagot, R.C., van Hasselt, F.N., Champagne, D.L., Meaney, M.J., Krugers, H.J., and Joëls, M. (2009). Maternal care determines rapid effects of stress mediators on synaptic plasticity in adult rat hippocampal dentate gyrus. Neurobiol. Learn. Mem. *92*, 292–300.

46. Jiang, X., Tian, Q., Wang, Y., Zhou, X.W., Xie, J.Z., Wang, J.Z., and Zhu, L.Q. (2011). Acetyl-L-carnitine ameliorates spatial memory deficits induced by inhibition of phosphoinositol-3 kinase and protein kinase C. J. Neurochem. *118*, 864–878.

47. Orr, A.G., Hsiao, E.C., Wang, M.M., Ho, K., Kim, D.H., Wang, X., Guo, W., Kang, J., Yu, G.Q., Adame, A., et al. (2015). Astrocytic adenosine receptor A2A and Gs-coupled signaling regulate memory. Nat. Neurosci. *18*, 423–434.

YMTHE, Volume *25*

Supplemental Information

Targeting the HDAC2/HNF-4A/miR-101b/AMPK Pathway Rescues Tauopathy and Dendritic Abnormalities in Alzheimer's Disease

Dan Liu, Hui Tang, Xin-Yan Li, Man-Fei Deng, Na Wei, Xiong Wang, Ya-Fan Zhou, Ding-Qi Wang, Peng Fu, Jian-Zhi Wang, Sébastien S. Hébert, Jian-Guo Chen, Youming Lu, and Ling-Qiang Zhu

Supplementary Figures

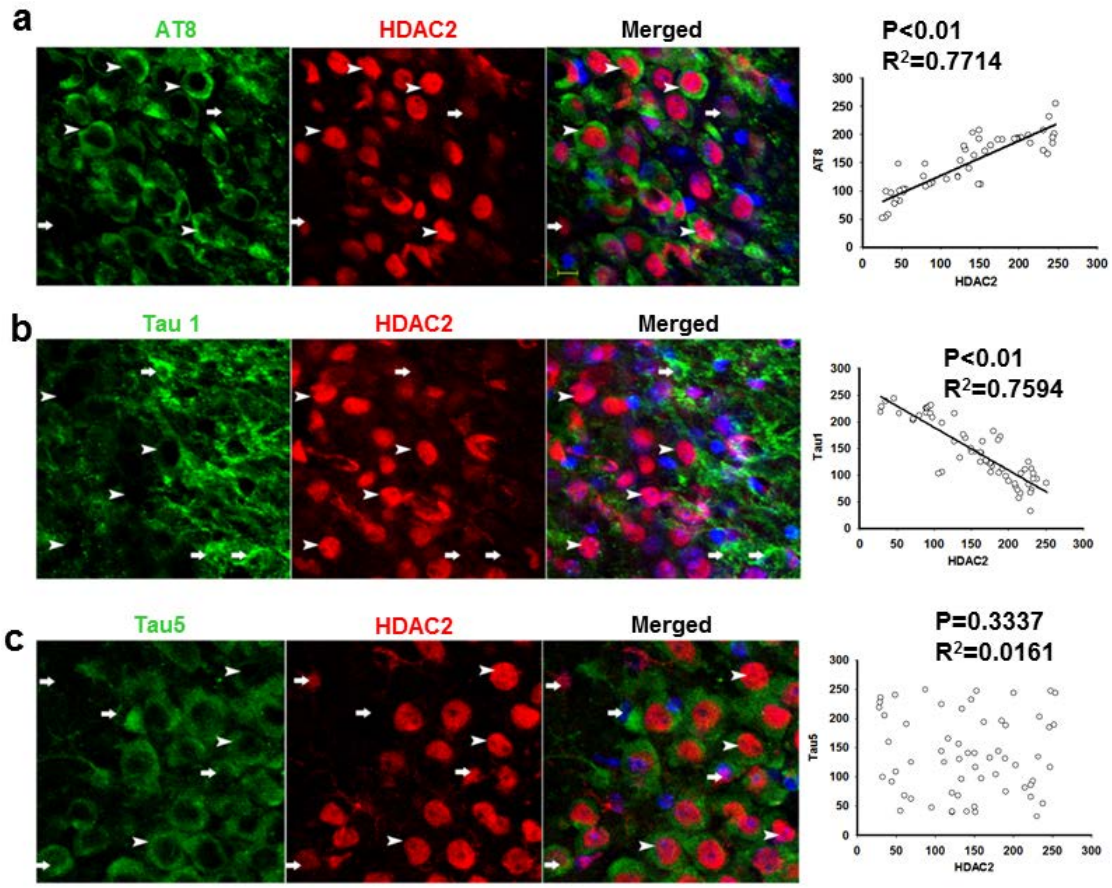

Fig. S1. HDAC2 expression is correlated with tau phosphorylation in P301L Tau mice

(a) The double immunofluorescence were performed in the 9-month P301L Tau mice hippocampal slices by using the AT8 (Green) and HDAC2 (Red) antibodies and the correlation analysis was performed by Sigmaplot after the fluorescent intensity measurement by Image J. Arrowhead, neurons with high level of HDAC2 intensity; Arrow, neurons with low level of HDAC2 intensity. N=52.

(b) The double immunofluorescence were performed in the 9-month P301L Tau mice hippocampal slices by using the Tau1 (Green) and HDAC2 (Red) antibodies and the correlation analysis was performed by Sigmaplot after the fluorescent intensity

measurement by Image J. Arrowhead, neurons with high level of HDAC2 intensity; Arrow, neurons with low level of HDAC2 intensity. N=58.

(c) The double immunofluorescence were performed in the 9-month P301L Tau mice brain slices by using the Tau5 (Green) and HDAC2 (Red) antibodies and the correlation analysis was performed by Sigmaplot after the fluorescent intensity measurement by Image J. Arrowhead, neurons with high level of HDAC2 intensity; Arrow, neurons with low level of HDAC2 intensity. N=55.

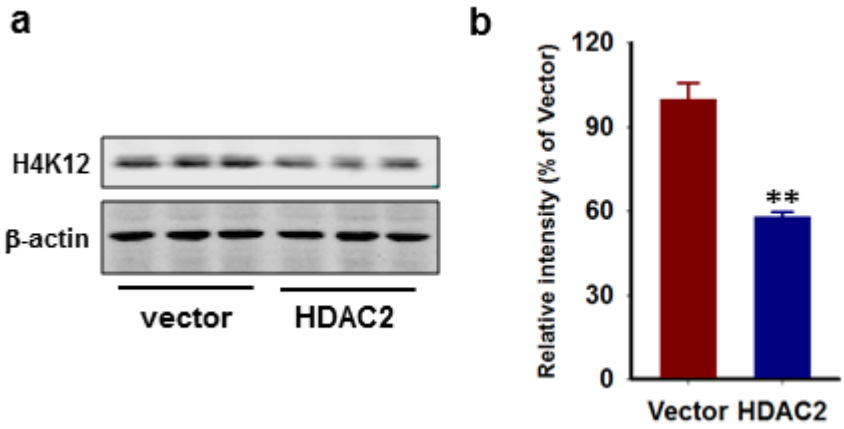

Fig. S2. Overexpression of HDAC2 reduces the acetylation of histone 4 at lysine 12 site.

(a, b) The hippocampal neurons were cultured to 14 DIV and then infected with lenti-HDAC2 (HDAC2) or vector control (vector) viruses. 48 hours later, the neurons were harvest and the cell lyses were used for western blot by the indicated antibodies. The representative images were shown in (a) and the quantitative analysis were performed (b). ** *P<0.01*, *vs.* Vector. N=4.

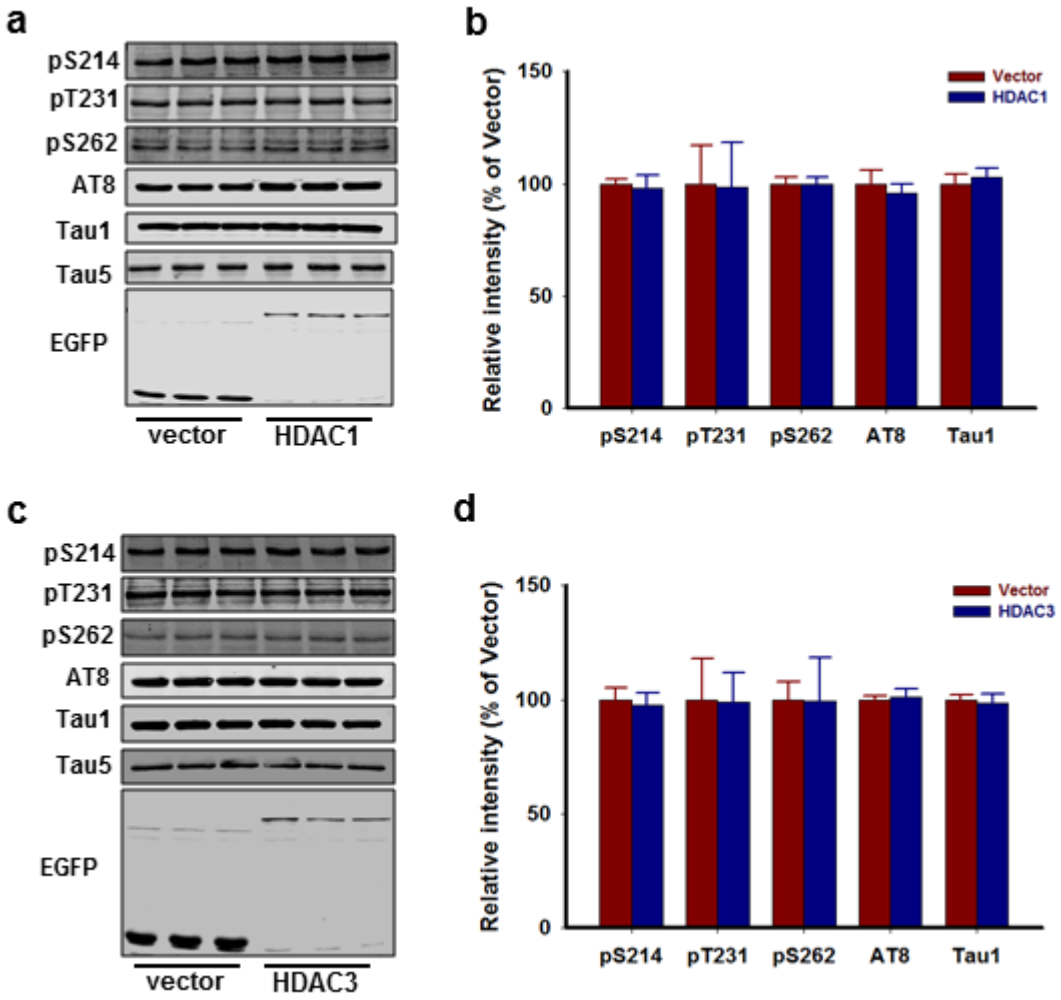

Fig. S3. Overexpression HDAC1 or HDAC3 does not induce the tauopathy *in vitro*

(a, b) The hippocampal neurons were cultured to 14 DIV and then infected with lenti-HDAC1 (HDAC1) or vector control (vector) viruses. 48 hours later, the neurons were harvest and the cell lyses were used for western blot by the indicated antibodies pS214, pT231, pS262, AT8, Tau1 and Tau5. The representative blots were shown in (a) and the quantitative analysis were performed in (b).

(c, d) The hippocampal neurons were cultured to 14 DIV and then infected with lenti-HDAC3 (HDAC3) or vector control (vector) viruses. 48 hours later, the neurons

were harvest and the cell lyses were used for western blot by the indicated antibodies pS214, pT231, pS262, AT8, Tau1 and Tau5. The representative blots were shown in (c) and the quantitative analysis were performed in (d).

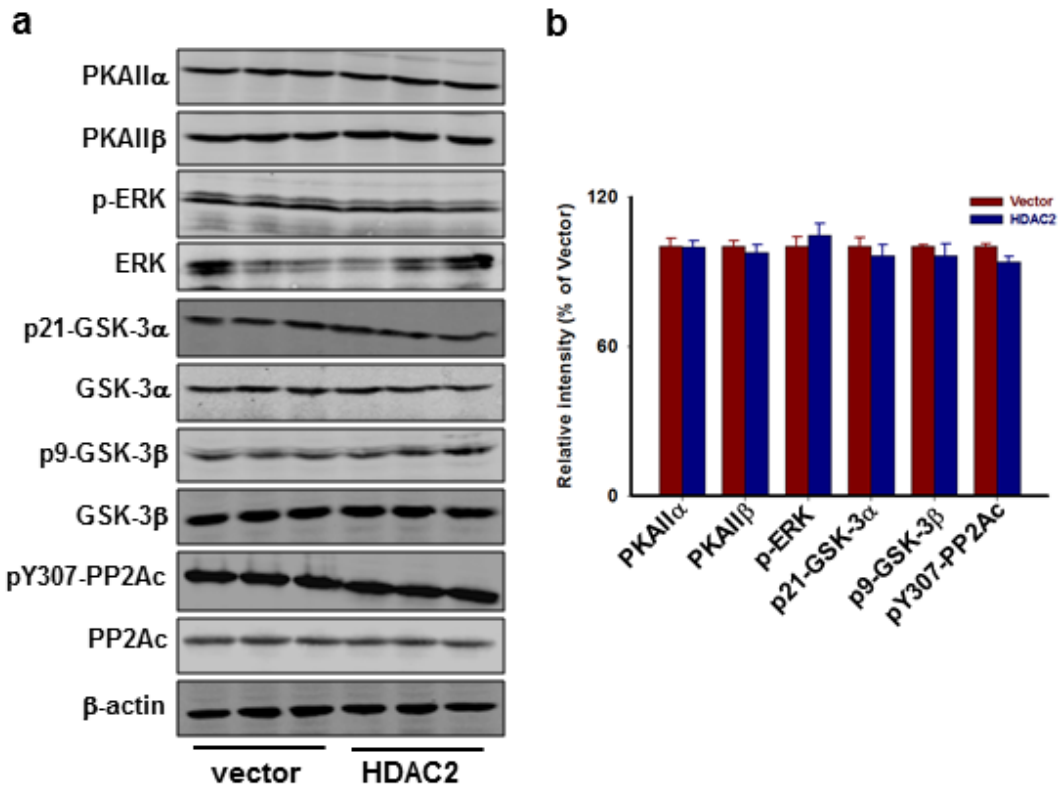

Fig. S4. Overexpression HDAC2 does not alter the activities of PKA, ERK, GSK-3α/β and PP2Ac *in vitro*

(a, b) The hippocampal neurons were cultured to 14 DIV and then infected with lenti-HDAC2 (HDAC2) or vector control (vector) viruses. 48 hours later, the neurons were harvest and the cell lyses were used for western blot by the indicated antibodies above. The representative blots were shown in (a) and the quantitative analysis were performed in (b).

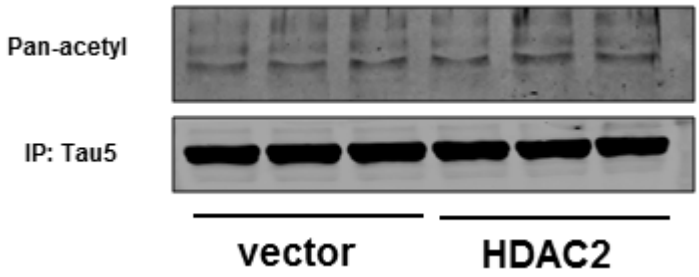

Fig. S5. Overexpression HDAC2 does not alter the acetylation of tau *in vitro*

The hippocampal neurons were cultured to 14 DIV and then infected with lenti-HDAC2 (HDAC2) or vector control (vector) viruses. 48 hours later, the neurons were harvest and the cell lyses were immunoprecipated with Tau 5 and then the pellets were immunoblotted by pan-acetylation antibody.

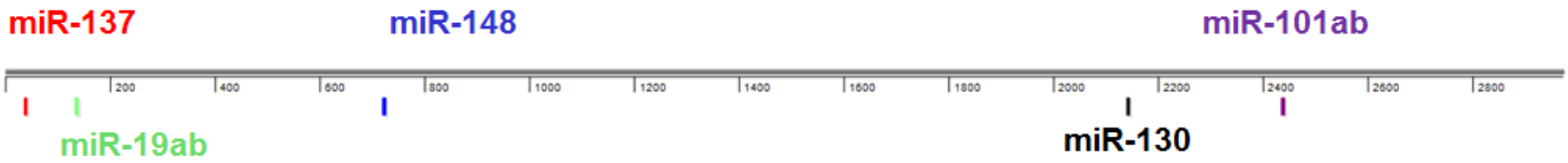

Fig. S6. The predicted binding sites of miRNAs in the 3'UTR of *PRKAA1*.

The 3'UTR sequence of *PRKAA1* was input to the Seqbuilder (Lasergene 7.0) and the different binding sites of predicted miRNAs were indicated.

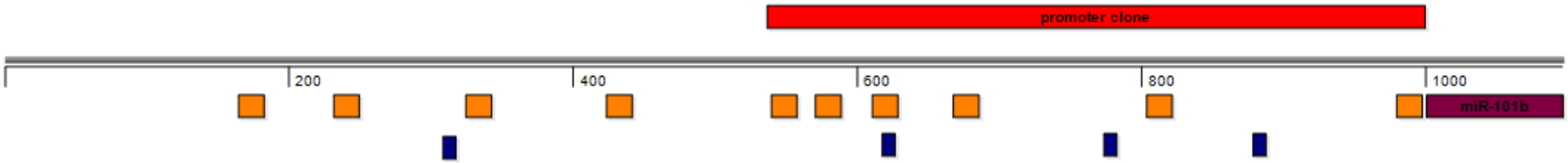

Fig. S7. The predicted binding sites of HNF-4A and Sox5 transcptional factor in the upstream of pri-miR-101b.

The upstream 1000 bp sequence of pri-miR-101b was input to the Seqbuider (Lasergene 7.0). The pri-miR-101b was labeled as purple color; the

cloned promoter sequence in luciferase experiment was labeled as red color. The predicted HNF-4A and Sox5 binding motifs were labeled as yellow color and blue color separatedly.

Supplementary Table 1: Potential binding sites of miR-101 promoter region that predicted by Motifmap

Location	+/-	BBLS	BLS	NLOD	Z-Score	FDR	Motif ID	TF Name	Gene	Distance	Region
chr19:29209757..29209763	+	6.183	7.815	1	3.683	0.176	M01033	HNF4	Mir101b	-11	Upstream
chr19:29209667..29209687	-	0	0.161	0.789	4.302	0.444	M01655	P53	Mir101b	-81	Upstream
chr19:29209634..29209640	-	1.049	2.613	1	4.476	0.471	MA0004	Arnt	Mir101b	-128	Upstream
chr19:29209634..29209640	+	1.049	2.613	1	4.476	0.471	MA0004	Arnt	Mir101b	-134	Upstream
chr19:29209495..29209503	+	2.113	3.181	1	4.232	0.012	M00712	myogenin	Mir101b	-273	Upstream
chr19:29209295..29209305	+	1.764	2.828	1	4.02	0.082	M01734	NFAT3	Mir101b	-473	Upstream
chr19:29209146..29209152	-	1.236	2.453	1	4.476	0.477	MA0004	Arnt	Mir101b	-616	Upstream
chr19:29209146..29209152	+	1.236	2.453	1	4.476	0.477	MA0004	Arnt	Mir101b	-622	Upstream
chr19:29209105..29209125	+	0	0.512	0.817	4.512	0.213	M01200	CTCF	Mir101b	-663	Upstream
chr19:29209006..29209013	+	3.06	5.394	1	3.688	0.495	M01131	SOX10	Mir101b	-762	Upstream
chr19:29208765..29208777	-	0.007	0.161	0.91	4.421	0.363	MA0141	Esrrb	Mir101b	-991	Upstream
chr19:29208762..29208774	-	0.012	0.161	0.909	4.537	0.081	M01589	ERR2 (ESF	Mir101b	-994	Upstream
chr19:29208765..29208771	-	4.625	5.435	1	3.591	0.058	M01032	HNF4	Mir101b	-997	Upstream
chr19:29208617..29208623	-	1.666	2.566	1	3.683	0.171	M01033	HNF4	Mir101b	-1145	Upstream
chr19:29208539..29208546	-	0.927	1.314	1	4.148	0.087	M00468	AP-2rep	Mir101b	-1222	Upstream
chr19:29208536..29208542	-	0.978	1.314	1	3.683	0.171	M01033	HNF4	Mir101b	-1226	Upstream
chr19:29208253..29208261	-	1.402	1.675	1	3.771	0.379	M00494	STAT6	Mir101b	-1507	Upstream
chr19:29208197..29208204	-	1.365	1.513	1	3.958	0	MA0087	SOX5	Mir101b	-1564	Upstream
chr19:29208096..29208111	+	0.012	0.541	0.843	4.377	0.413	M00495	Bach1	Mir101b	-1672	Upstream
chr19:29208091..29208100	+	0.008	0.161	0.941	4.398	0.154	M01139	LMAF	Mir101b	-1677	Upstream
chr19:29208083..29208095	+	0.396	0.996	0.963	4.68	0.125	M01142	LRH1	Mir101b	-1685	Upstream
chr19:29207921..29207935	+	0.003	0.161	0.881	4.42	0.368	M01185	BCL6	Mir101b	-1847	Upstream

Supplementary Table 2. Potential binding sites of miR-101 promoter region that predicted by TFbind

Supplementary Table 3. Primary antibodies used in current study

Antibodies	Type	WB dilution	IHC dilution	References and sources
Tau1	mAb	-	1:200	Millipore (Billerica, MA, USA)
AT8	mAb	-	1:100	Thermo
HDAC2	mAb	1:1000	1:100	Abcam (Cambridge, UK)
pT231	pAb	1:1000	-	SAB (Pearland, TX, USA)
pS214	pAb	1:500	-	SAB (Pearland, TX, USA)
pT262	pAb	1:500	-	SAB (Pearland, TX, USA)
Tau5	mAb	1:1000	-	Thermo
EGFP	pAb	1:1000	-	Abcam (Cambridge, UK)
DM1A	mAb	1:1000	-	Sigma (St. Louis, MO, USA)
GSK-3β	pAb	1:1000	-	SAB (Pearland, TX, USA)
pS9-GSK-3β	pAb	1:1000	-	Cell Signaling (Danvers, MA, USA)
GSK-3α	pAb	1:1000	-	SAB (Pearland, TX, USA)
pS21-GSK-3α	pAb	1:1000	-	Cell Signaling (Danvers, MA, USA)
PP2ac	mAb	1:1000	-	Millipore (Billerica, MA, USA)
pY307-PP2ac	pAb	1:1000	-	Abcam (Cambridge, UK)
Ace-H4K12	pAb	1:1000		Abcam (Cambridge, UK)
CDK5	mAb	1:1000	-	Santa Cruz, CA, USA
P35/25	pAb	1:1000	-	Santa Cruz, CA, USA
PKAα	pAb	1:1000	-	Santa Cruz, CA, USA
PKAβ	pAb	1:1000	-	Santa Cruz, CA, USA
p-ERK	pAb	1:1000	-	Cell Signaling (Danvers, MA, USA)
ERK	pAb	1:1000	-	Cell Signaling (Danvers, MA, USA)
Pan-acetylation	pAb	1:1000		Cell Signaling (Danvers, MA, USA)
HNF-4A	pAb	1:1000		Sigma (St. Louis, MO, USA)
pS304-HNF-A	pAb	1:500		SAB (Pearland, TX, USA)
AMPK	pAb	1:1000		Abcam (Cambridge, UK)
Goat-anti- mouse -peroxidase	-	1:5,000	-	Pierce Chemical Company
Goat-anti- rabbit -peroxidase	-	1:5,000	-	Pierce Chemical Company